



Evaluation of US and MRI techniques for carotid stenosis: a novel phantom approach

Lilla Bonanno² · Silvia Marino^{1,2} · Rosa Morabito^{2,3} · Giancarlo Barbalace⁴ · Angela Sestito⁵ · Barbara Testagrossa¹ · Giuseppe Acri¹ 

Received: 27 July 2017 / Accepted: 5 December 2018 / Published online: 12 December 2018
© Italian Society of Medical Radiology 2018

Abstract

Carotid atherosclerosis is very important in the pathogenesis of cerebral ischemia. Ultrasonography (US) and magnetic resonance imaging (MRI) are the predominant noninvasive techniques capable to identify the presence and stage of intra-plaque hemorrhage. In this work, we propose a novel dedicated phantom that can be used for both US and MRI scanners to evaluate carotid atherosclerotic lesions. The phantom consists of a polymethyl metacrylate (PMMA) diagonally crossed by a PMMA hollow cylinder simulating a blood vessel. To simulate a stenosis, we inserted a plastic hollow tube inside the cylinder. Quantitative image analysis, based on accuracy measurements, was performed on two US and two MRI scanners. The accuracy measurements have highlighted the use of the 3.0 T MRI scanner to characterize the vessel stenosis. However, no significant difference between US and MRI techniques was found in Fisher exact test and inter-rater agreement. The concordance correlation coefficient showed a moderate agreement between some methods. Agreement between 3.0 T and other methods results poor, and this could be due to the fact that the 3.0 T has a better resolution compared to a US and MR 1.5 T. These methods seem to have similar efficacies for the evaluation of vessel stenosis, legitimizing the use of the developed phantom as a versatile and reproducible instrument that could be used during quality controls programs.

Keywords Carotid atherosclerosis diagnosis · Ultrasound · Magnetic resonance imaging · Quality controls

Introduction

Atherosclerosis is a chronic disease that affects medium and large arteries. The resultant plaque can obstruct lumen or disseminate material into blood stream and could be a cause of myocardial infarction, stroke and peripheral vascular disease [1].

In particular, carotid atherosclerosis is very important in the pathogenesis of cerebral ischemia [2]. Although advances in the understanding and treatment of these lesions

have been performed, thrombotic complications of atherosclerosis remain one of the most important causes of morbidity and mortality in Western society [3].

It should be important to have a noninvasive imaging technique capable to identify, not only the presence, but also the stage of intra-plaque hemorrhage. Currently, the predominant noninvasive imaging modalities investigated for this purpose are (a) ultrasonography (US) and (b) magnetic resonance imaging (MRI) techniques [4].

In particular, US and MRI are highly sophisticated imaging modalities for an accurate and timely diagnosis [2, 5, 6]. MRI utilizes powerful static magnetic fields to align the magnetic spins of the protons in water molecules and to drive the Larmor precession which provides the signal used to construct the image [7], whereas the principle of ecography is similar to that of sonar or radar; in essence, following an US pulse transmission, echoes from the medium being interrogated are detected and used to form an image [8].

These US waves are transmitted from probe to body, and the signal is reflected wherever there is an interface between two tissues with different acoustic impedances. In

✉ Giuseppe Acri
gacri@unime.it

¹ Department of BIOMORF, University of Messina, Messina, Italy

² IRCCS Centro Neurolesi “Bonino-Pulejo”, Messina, Italy

³ Biomedical Department of Internal and Specialistic Medicine, University of Palermo, Palermo, Italy

⁴ Casa di Cura “Cristo Re”, Messina, Italy

⁵ High School Campo Calabro (RC), Campo Calabro, Italy

this context, color or power Doppler US is a simple and non-invasive method used to characterize carotid atherosclerotic lesions, using echogenicity, even if it depends on operator and patient.

For this reason, there are circumstances where an alternative carotid arteries MRI imaging modality has been reported to characterize plaque components of lipid cores, intra-plaque hemorrhage, fibrosis, and calcification [9–12]. It should be possible to differentiate soft and unstable plaques with liquid constituents from solid, hard, and stable plaques.

These diagnostic modalities are based on acquisition and correct evaluation of images. Underhill [13], Crowe [14] and Mani [15] were the first who investigated the relation between carotid MRI and US.

In any case, it is important to guarantee the maintenance of the consistent image quality of the radiological equipments. For this reason, in the clinical imaging study, it is important to have accurate confirmation of several physical characteristics of the medical imaging device. In this context, quality controls (QC) have an important role because QC enables a complete evaluation of system status and image quality [16–18] and permit the identification of image quality degradation and source of possible equipment malfunction [5, 19]. In fact, the purpose of QC testing is to detect changes that may result in a clinically significant degradation in image quality [20] which reduces the ability to detect and correctly interpret abnormal findings.

For this reason, the optimization of image reproducibility motivates the calibration of acquisition protocols that use phantoms with defined dimensions, inserts etc.

Phantoms are usually used in order to guarantee the maintenance of consistent image quality over lifetime of the diagnostic equipment.

In this context, to geometrically characterize carotid atherosclerotic lesions, diameter stenosis percentage and area stenosis percentage have to be determined. Therefore, accuracy of stenosis size represents a significant parameter that should be estimated during QC, to correctly evaluate area stenosis percentage.

However, most US and MRI scanners adopt specific automated procedures that require the use of dedicated phantoms. Usually, these phantoms are different for the two

modalities and require specific protocols depending also on specific diagnostic device [21–23].

Recently, we realized a single polymethyl methacrylate (PMMA) phantom that was suitable to perform quality inspection both on CT and on MRI that may be used to provide a complete quality inspection of a CT and MRI equipment [24]. On the basis of this experience, we propose a novel dedicated phantom easy to implement which can be used on both US and MRI scanners. In this work, we performed a US and MRI examination, by using the novel phantom, for a qualitative and quantitative stenosis evaluation.

The reliability of this study was evaluated by a detailed statistical analysis. In particular, Fisher exact test (*F* test) and concordance correlation coefficient (CCC) were used: the *F* test was useful to assess whether a significant difference existed between data sets that were obtained following different procedures, while the CCC test was important in order to assess agreement and concordance between the MRI and US methods.

Materials and methods

Phantom

This novel dedicated phantom consists of a PMMA empty box (18.0 cm × 28.5 cm × 18.0 cm) diagonally crossed by a PMMA hollow cylinder, oriented at 26.84° across the beam width, simulating a blood vessel. The parameters that characterize the blood vessel are: diameter 5 mm and thickness 1 mm. In order to mimic the US and MRI characteristics of a stenosis, we inserted a thin semirigid plastic wall. This wall is a hollow tube (3.0 mm × 0.8 mm), inside the hollow cylinder (Fig. 1), which mimics an area stenosis percentage of 36%. The choice of PMMA and semirigid plastic tubing was related to the necessity of using no ferromagnetic elements in order to perform geometric stenosis measurements both on an MRI scanner and on an US device. In previous works, stenosis models with different diameter and/or area reductions have been manufactured in order to study the effect of the degree of stenosis and flow rate in large vessels in CT, MRI and US [21–23], but no comparison among different

Fig. 1 Upper and lateral view of the phantom

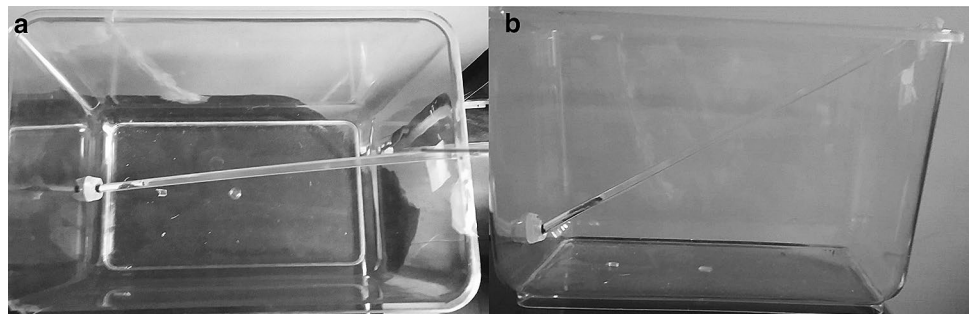


Table 1 Physical and acoustic properties of blood mimicking fluid compared with the human blood

Properties	Human blood (37 °C)	Blood mimicking fluid (22 °C)
Scatterer	Red blood cells	Orgasol™ (nylon)
Scatterer size (µm)	7	5
Density (kg m ⁻³)	1053	1035 ± 5
Velocity (m s ⁻¹)	1583	1550 ± 15
Attenuation (dB cm ⁻¹ MHz ⁻¹)	0.15	0.07 ± 0.05
Viscosity (mPa s)	3	4 ± 1
Fluid properties	Non-Newtonian	Newtonian

Table 2 Parameters that characterize the blood vessel and simulate stenosis

Parameters	Measures
Blood vessel	
Thickness	1.0 mm
Diameter	5.0 mm
Simulate stenosis	
Thickness	0.8 mm
Diameter	3.0 mm
Angle	26.84°

diagnostic devices was performed. In particular, models which mimicked area stenosis in large vessels ranging from 18% up to 90% were made.

The PMMA box was filled with distillate water, while the hollow cylinder was filled with a liquid solution, mimicking human blood, and containing: water, glycerol, orgasol, detergents, citric acid and Acnibio OCS (Dansk Fantom Service). Orgasol, characterized by nylon particles 5 µm in diameter, has been used in blood mimicking fluids when natural buoyancy of the particles has been achieved, whereas glycerol avoids refraction [25–27]. The presence of other elements guarantees long-time preserving of the fluid. The solution was diluted with distillate water (1:9 in volume), following the manufacturer's indication, in order to guarantee the same

characteristics (e.g., viscosity, acoustic properties) of human blood, as indicated in Table 1. All the geometric parameters that characterize the novel developed phantom are reported in Table 2.

US and MRI data acquisition

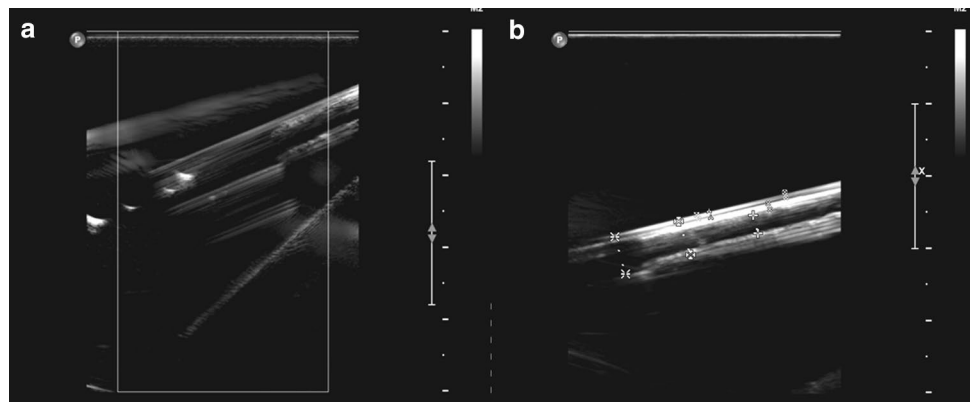
The common carotid artery (CCA) US data were obtained as longitudinal cross sections using two different US devices: a Philips iU22 US and a Philips iE33 system. In both US systems, a broadband linear L9-3 probe, operating in 3–9 MHz frequency range, was used. The L9-3 probe can be utilized for vascular (carotid, arterial and venous) and superficial imaging applications.

In this case, vascular carotid preset on the machine was used (Vasc Car preset, persistence low, XRES and SONOCT on) and the gain was optimized by the operator who is an experienced vascular sonographer.

The best images are still captured and stored in the Digital Imaging and Communications in Medicine (DICOM) file format for further evaluation, and the selected ones were qualitatively and quantitatively analyzed using the owner software of the US devices (Fig. 2).

The MRI data were obtained using two different scanners that are characterized by a different static magnetic field values, 1.5 T and 3.0 T, respectively (Fig. 3). In both cases, the sequences we considered were a T1-weighted turbo spin echo (T1w TSE) sequence and a T2-weighted turbo spin echo (T2w TSE) one. In fact, the T2w TSE and T1w TSE weighting was essential for plaque assessment and identification of calcification. In addition, a T2 spectral presaturation with inversion recovery (T2 SPIR) sequence was also considered in order to suppress fat and reconstruct carotid artery wall [28–30]. All the scan parameters are indicated in Table 3.

Also in this case, the MRI DICOM images were acquired and directly analyzed using the owner software of the MRI devices.

Fig. 2 US images of the novel dedicated phantom. **a** Longitudinal cross section; **b** longitudinal cross section and measurements performed

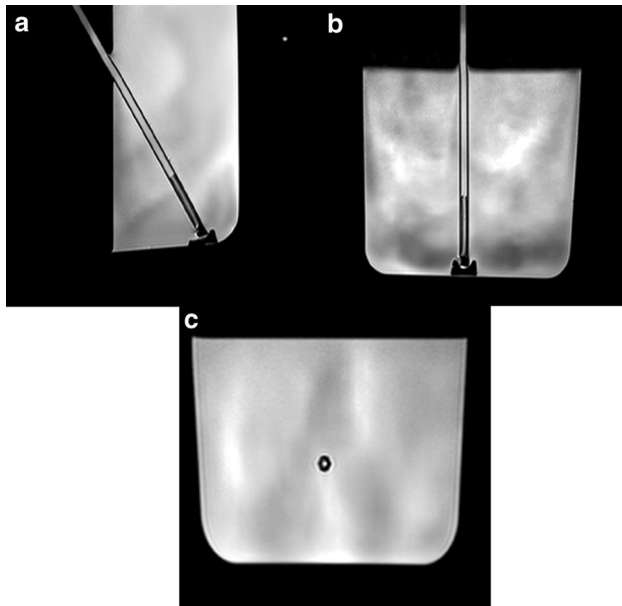


Fig. 3 MRI images of novel dedicated phantom. **a** sagittal; **b** coronal; **c** axial

Table 3 MRI (1.5 T and 3.0 T) scan parameters

Sequence	T2W_TSE	T1W_TSE	TT2 SPIR SAG
Slice thickness	3	4	3.5
Time repetition	3500	400	2000
Echo time	120	7,5	60
Echo numbers	1	1	1
Interslice gap	3.3	4.4	3.85
Reconstruction diameter	250	300	290

All the US and MRI images were acquired in static conditions, i.e., the effect of the blood flow was negligible.

In both cases, the parameters that we consider for measurements are: filter vessel, diameter vessel, filter stenosis, diameter and angle stenosis.

Image measurements and statistical analysis

Three raters, neurovascular expert with more than 3 years of clinical experience analyzed US and MRI images using the owner software of the devices. The raters were blinded from information of phantom. Blood vessel diameter, blood vessel thickness, simulate stenosis thickness, simulate stenosis diameter and angle were manually segmented.

Accuracy measurements, using Eq. (1), were performed to assess whether the developed phantom could be used on both MRI and US devices.

$$\text{Accuracy (\%)} = \left| \frac{x_{\text{meas}} - x_{\text{ref}}}{x_{\text{ref}}} \right| \times 100 \quad (1)$$

where x_{meas} represents the measured values and x_{ref} indicates the reference ones.

Later, a parametric analysis was carried out because the results of the Shapiro–Wilk normality test indicated that most of the target variables were normally distributed. Analysis of variance, using F test was performed, to assess whether a significant difference existed among the different data sets. The F test is highly used when the aim of the study is to evaluate a precision of a measurement technique. In fact, analysis of variance consists of factorization of the total variance into a set of partial variances, which correspond to different and estimated variations. For continuous data, the CCC was used, to assess the agreement between two methods (MRI 1.5 T and 3.0 T; US iU22 and iE33) and to assess the concordance between MRI and US methods. The concordance correlation coefficient combines measures of precision and accuracy, to determine how the observed data deviate from the line of perfect concordance (line at 45° on a square scatter plot). Intra-rater analysis was used to determine test rest-reliability, comparing the different scores marked by the same rater on the same phantom with different methods.

Finally, inter-rater agreement was assessed between the various measurements obtained with the different techniques in order to test the performance stability with different raters. Inter-rater agreement was estimated through intra-class correlation coefficients (ICC), one-way analysis of variance with random effects. The maximum ICC value is 1.00, and it represents the stronger reliability. In general, ICC values above 0.75 indicate a good reliability. Analyses were performed using an open-source R3.0 software package (<http://www.r-project.org>). A 95% of confidence level was set with a 5% alpha error. Statistical significance was set at $p < 0.05$.

Results

Accuracy measurements

In Tables 4 and 5, the results of the measurements, respectively, conducted on US and MRI devices are reported. All the parameters that characterized the novel phantom have been evaluated.

Fisher's exact test

In Tables 6 and 7, continuous variables were expressed as mean \pm standard deviation. The F test was used to verify whether data sets were comparable. For iU22 and iE33 US data, we did not obtain statistically significant difference between the two methodologies (Table 6). For 1.5 T and 3.0 T MRI, we did not obtain statistically significant difference between the two methodologies (Table 7).

Table 4 Accuracy measurements conducted on US devices

Parameters	iU22 L9-3		iE33 L9-3	
	Mean	Accuracy (%)	Mean	Accuracy (%)
Blood vessel				
Thickness (mm)	0.99	1.00	0.99	1.00
Diameter (mm)	4.93	1.40	4.92	1.60
Simulate stenosis				
Thickness (mm)	0.89	11.25	0.89	11.25
Diameter (mm)	2.80	6.67	2.82	6.00
Angle (°)	29.83	11.14	29.77	10.92

Table 5 Accuracy measurements conducted on MRI devices

Parameters	1.5 T		3.0 T	
	Mean	Accuracy (%)	Mean	Accuracy (%)
Blood vessel				
Thickness (mm)	1.05	5.00	1.0	0.00
Diameter (mm)	4.94	1.20	5.0	0.00
Simulate stenosis				
Thickness (mm)	0.95	18.75	0.97	21.25
Diameter (mm)	2.8	6.67	2.9	3.33
Angle (°)	27.83	3.69	29.0	8.05

Table 6 US images results

Parameters	iU22 L9-3	iE33 L9-3	<i>F</i>	<i>p</i>
	Mean ± SD	Mean ± SD		
Blood vessel				
Thickness (mm)	0.99 ± 0.01	0.99 ± 0.01	1.33	0.86
Diameter (mm)	4.93 ± 0.06	4.92 ± 0.07	1.69	0.74
Simulate stenosis				
Thickness (mm)	0.89 ± 0.01	0.89 ± 0.01	0.57	0.73
Diameter (mm)	2.80 ± 0.17	2.82 ± 0.21	1.57	0.78
Angle (°)	29.83 ± 0.29	29.77 ± 0.58	4	0.4

Concordance correlation coefficient

The CCC showed a moderate agreement between some methods (Table 8). In US (iU22 and iE33), we obtained a moderate/high agreement for blood vessel CCC = 0.84 (−0.42 to 0.99) and for simulate stenosis CCC = 0.94 (0.40; 0.99) diameter; in 1.5 T and iU22 for blood vessel diameter CCC = 0.97 (0.35; 0.99); in 1.5 T and iE33 for blood vessel diameter CCC = 0.86 (0.006–0.99) and for simulate stenosis diameter CCC = 0.94 (0.40; 0.99). Agreement between 3.0 T and other methods results poor, and this could be due to the fact that the 3.0 T has a better resolution compared to US and MR 1.5 T.

Table 7 MRI images results

Parameters	1.5 T	3.0 T	<i>F</i>	<i>p</i>
	Mean ± SD	Mean ± SD		
Blood vessel				
Thickness (mm)	1.05 ± 0.22	1.0 ± 0.10	0.21	0.35
Diameter (mm)	4.94 ± 0.05	5.0 ± 0.10	3.57	0.44
Simulate stenosis				
Thickness (mm)	0.95 ± 0.13	0.97 ± 0.06	0.19	0.32
Diameter (mm)	2.8 ± 0.10	2.9 ± 0.10	1	1
Angle (°)	27.83 ± 1.53	29.0 ± 1.0	0.43	0.6

Inter-rater agreement

For inter/RR, ICC was calculated to evaluate the consistency of parameters considering different raters. In Table 9, we reported the resulting ICCs for the three comparison conditions for the different techniques. The results obtained by intra-rater agreement to compare two techniques are significant. We obtained a moderate/high agreement in 1.5T, iU22 and iE33. For the 3.0T MRI measurements, we observed that high agreement in all ICC values is > 0.90.

Discussion

Qualitative classification of vessel stenosis, which highly depends on medical staff capability, and its quantitative characterization are crucial in the diagnosis and treatment planning. In this study, we assess the diagnostic ability of US and MRI techniques to identify and measure carotid stenosis.

In order to choose a method for investigation, different parameters should be considered: availability of modality, level of optimization and the capability of patient and operator. For neurological research, MRI is usually preferred. US is the cheapest and safest modality, but it is operator-dependent. MRI is an expensive technique and it is not present in most of the hospitals.

It is important to consider that US is more available than MRI. Thus, it is used more frequently than MRI as a screening modality. On the other hand, by using MRI it is possible to acquire tridimensional images with the high contrast resolution.

Other authors have conducted studies about the use of dedicated phantoms to evaluate stenosis parameter [21–23], but no comparison between diagnostic devices was performed. This is a first study that reports a comparison among two different US modalities and two different MRI strength fields (1.5 and 3 T) with a novel phantom approach.

In this context, we developed a novel phantom, simulating a vessel stenosis that can be used both on MRI and on US devices. The phantom mimics the anatomical

Table 8 Concordance correlation coefficient values (95% confidence intervals)

	Blood vessel		Simulate stenosis		Angle
	Thickness	Diameter	Thickness	Diameter	
1.5T–3.0T	0.65 (–0.11; 0.93)	0.55 (–0.30; 0.91)	0.47 (–0.61; 0.94)	0.57 (–0.29; 0.92)	0.56 (–0.29; 0.91)
iU22–iE33	0.80 (–0.53; 0.99)	0.84 (–0.42; 0.99)	0.73 (–0.70; 0.99)	0.94 (0.40; 0.99)	0.73 (0.19; 0.99)
1.5T–iU22	0.07 (–0.02; 0.17)	0.97 (0.35; 0.99)	0.15 (–0.12; 0.40)	0.77 (–0.25; 0.98)	0.08 (–0.14; 0.29)
1.5T–iE33	0.09 (–0.002; 0.19)	0.86 (0.006; 0.99)	0.13 (–0.06; 0.31)	0.94 (0.40; 0.99)	0.17 (–0.28; 0.57)
3.0T–iU22	0.2 (0.13; 0.26)	0.5 (–0.43; 0.91)	0.13 (0.16; 0.40)	0.54 (–0.42; 0.93)	0.23 (–0.26; 0.64)
3.0T–iE33	0.19 (–0.04; 0.41)	0.61 (–0.26; 0.93)	0.05 (–0.16; 0.25)	0.63 (0.12; 0.92)	0.5 (–0.43; 0.91)

Table 9 Inter-class correlation coefficient values (95% confidence intervals)

	Blood vessel		Simulate stenosis		Angle
	Thickness	Diameter	Thickness	Diameter	
1.5T	0.88 (–0.31; 0.99)	0.92 (0.21; 0.99)	0.89 (–0.17; 0.99)	0.92 (0.13; 0.99)	0.97 (0.68; 0.99)
3.0T	0.97 (0.64; 0.99)	0.92 (0.14; 0.99)	0.95 (0.44; 0.99)	0.97 (0.71; 0.99)	0.94 (0.40; 0.99)
iU22 L9-3	0.83 (–0.82; 0.99)	0.92 (0.18; 0.99)	0.89 (–0.18; 0.99)	0.96 (0.60; 0.99)	0.86 (–0.43; 0.99)
iE33 L9-3	0.81 (–1.05; 0.99)	0.96 (0.56; 0.99)	0.87 (–0.40; 0.99)	0.87 (–0.38; 0.99)	0.94 (0.36; 0.99)

characteristics of the obstructed vessel, as closely as possible, but remains simply to use and provides reproducible data. Its preparation requires only the filling of the hollow cylinder and the PMMA box, using, respectively, a solution, simulating human blood and distillate water.

The accuracy obtained using the 3 T device is significantly higher than that obtained using the other diagnostic scanners.

However, statistical analysis showed that no significant difference exist between US and MRI techniques. In fact, US and MRI have shown similar diagnostic efficacies for the evaluation of vessel stenosis, using the novel phantom. The obtained results showed that there was concordance between the two different diagnostic techniques; however, we found significant results in inter-rater agreement. In particular, high diagnostic agreement and good triage of rater agreement were found for MRI 3.0 T. This could be due to the fact that the 3.0 T magnet has the capability to provide a better image quality as the base for improved diagnostic performance, because doubling the field strength (almost) doubles signal-to-noise ratio, that is, the quantity of signal made available from the patient in order to build MRI images.

The proposed method employs a new universal phantom, which can be used on any US and MRI device, in a quick manner, to evaluate stenosis vessel. In addition, this developed methodology could represent a simple, versatile and reproducible instrument to evaluate new physical parameters for implementing routinely QC programs.

Compliance with ethical standards

Conflict of interest The authors declare that they have no conflict of interest.

Ethical approval This article does not contain any studies with human participants or animals performed by any of the authors.

References

- Cai JM, Hatsukami TS, Ferguson MS, Small R, Polissar NL, Yuan C (2002) Classification of human carotid atherosclerotic lesions with in vivo multicontrast magnetic resonance imaging. *Circulation* 106(11):1368–1373. <https://doi.org/10.1161/01.CIR.0000028591.44554.F9>
- Bonanno L, Sottile F, Ciurleo R, Di Lorenzo G, Bruschetta D, Bramanti A, Ascenti G, Bramanti P, Marino S (2017) Automatic algorithm for segmentation of atherosclerotic carotid plaque. *J Stroke Cerebrovasc Dis* 26(2):411–416. <https://doi.org/10.1016/j.jstrokecerebrovasdis.2016.09.045>
- Kampschulte A, Ferguson MS, Kerwin WS, Polissar NL, Chu B, Saam T, Hatsukami TS, Yuan C (2004) Differentiation of intraplaque versus juxtaluminar hemorrhage/thrombus in advanced human carotid atherosclerotic lesions by in vivo magnetic resonance imaging. *Circulation* 110(20):3239–3244. <https://doi.org/10.1161/01.CIR.0000147287.23741.9A>
- Yuan C, Mitsumori LM, Beach KW, Maravilla KR (2001) Carotid atherosclerotic plaque: noninvasive MR characterization and identification of vulnerable lesions. *Radiology* 221(2):285–299. <https://doi.org/10.1148/radiol.2212001612>
- Torfeh T, Beaumont S, Guédon JP, Normand N, Denis E (2007) Software tools dedicated for an automatic analysis of the CT

- scanner Quality Control's Images. In: Conf proc IEEE eng med biol soc. <https://doi.org/10.1117/12.707343>
6. Bonanno L, Marino S, Bramanti P, Sottile F (2015) Validation of a computer-aided diagnosis system for the automatic identification of carotid atherosclerosis. *Ultrasound Med Biol* 41(2):509–516. <https://doi.org/10.1016/j.ultrasmedbio.2014.09.004>
 7. Schenck JF (2005) Physical interactions of static magnetic fields with living tissues. *Prog Biophys Mol Biol* 87:185–204. <https://doi.org/10.1016/j.pbiomolbio.2004.08.009>
 8. Shung KK (2015) *Diagnostic ultrasound: imaging and blood flow measurements*, 2nd edn. CRC Press Taylor & Francis, Boca Raton
 9. Yuan C, Zhang SX, Polissar NL, Echelard D, Ortiz G, Davis JW, Ellington E (2002) Identification of fibrous cap rupture with magnetic resonance imaging is highly associated with recent transient ischemic attack or stroke. *Circulation* 105:181–185. <https://doi.org/10.1161/hc0202.102121>
 10. Moody AR, Murphy RE, Morgan PS, Martel AL, Delay GS, Allder S, MacSweeney ST, Tennant WG, Gladman J, Lowe J, Hunt BJ (2003) Characterization of complicated carotid plaque with magnetic resonance direct thrombus imaging in patients with cerebral ischemia. *Circulation* 107:3047–3052. <https://doi.org/10.1161/CIR.0000074222.61572.44>
 11. Serfaty JM, Chaabane L, Tabib A, Chevallier JM, Briguet A, Douek PC (2001) Atherosclerotic plaques: classification and characterization with T2-weighted high-spatial-resolution MR imaging—an in vitro study. *Radiology* 219:403–410. <https://doi.org/10.1148/radiology.219.2.r01ma15403>
 12. Ouhlous M, Flach HZ, de Weert TT, Hendriks JM, van Sambbek MRHM, Dippel DWJ, Pattynama PMT, van der Lugt A (2005) Carotid plaque composition and cerebral infarction: MR imaging study. *AJNR Am J Neuroradiol* 26:1044–1049
 13. Underhill HR, Kerwin WS, Hatsukami TS, Yuan C (2006) Automated measurement of mean wall thickness in the common carotid artery by MRI: a comparison to intima-media thickness by B-mode ultrasound. *J Magn Reson Imaging* 24:379–387. <https://doi.org/10.1002/jmri.20636>
 14. Crowe LA, Ariff B, Keegan J, Mohiaddin RH, Yang GZ, Hughes AD, McG Thom SA, Firmin DN (2005) Comparison between three-dimensional volume-selective turbo spin-echo imaging and two-dimensional ultrasound for assessing carotid artery structure and function. *J Magn Reson Imaging* 21:282–289. <https://doi.org/10.1002/jmri.20257>
 15. Mani V, Aguiar SH, Itskovich VV, Weinschelbaum KB, Postley JE, Wasenda EJ, Aguinaldo JGS, Samber DD, Fayad ZA (2006) Carotid black blood MRI burden of atherosclerotic disease assessment correlates with ultrasound intima media thickness. *J Cardiovasc Magn Reson* 8:529–534. <https://doi.org/10.1080/10976640600675245>
 16. Acri G, Tripepi MG, Causa F, Testagrossa B, Novario R, Vermiglio G (2012) Slice-thickness evaluation in CT and MRI: an alternative computerised procedure. *Radiol med* 17:507–518. <https://doi.org/10.1007/s11547-011-0775-5>
 17. Chen CC, Wan YL, Wai YY, Liu HL (2004) Quality assurance of clinical MRI scanners using ACR MRI phantom: preliminary results. *J Digit Imaging* 17:279–284. <https://doi.org/10.1007/s10278-004-1023-5>
 18. Goodsitt MM, Carson PL, Witt S, Hykes DL, Kofler JM Jr (1998) Real-time B-mode ultrasound quality control test procedures—report of AAPM ultrasound task group no. 1. *Med Phys* 25:1385–1406. <https://doi.org/10.1118/1.598404>
 19. Rampado O, Isoardi P, Ropolo R (2006) Quantitative assessment of computed radiography quality control parameters. *Phys Med Biol* 51:1577–1593. <https://doi.org/10.1088/0031-9155/51/6/015>
 20. Boone JM, Cody DD, Fisher JR, Frey GD, Glasser H, Gray JE, Haus AG, Hefner LV, Holmes RL Jr, Kobistek RJ, Ranallo FN, Rauch PL, Rossi RP, Seibert JA, Strauss KJ, Suleiman OH, Schenck JR, Thompson SK (2002) Quality control in diagnostic radiology. AAPM Report No 74
 21. Ramnarine KV, Anderson T, Hoskins PR (2001) Construction and geometric stability of physiological flow rate wall-less stenosis phantoms. *Ultrasound Med Biol* 27(2):245–250. [https://doi.org/10.1016/S0301-5629\(00\)00304-5](https://doi.org/10.1016/S0301-5629(00)00304-5)
 22. Nasiraei-Moghaddam A, Behrens G, Fatourae N, Agarwal R, Choi ET, Amini AA (2004) Factors affecting the accuracy of pressure measurements in vascular stenoses from phase-contrast MRI. *Magn Reson Med* 52:300–309. <https://doi.org/10.1002/mrm.20152>
 23. Yamada M, Jinzaki M, Kuribayashi S, Sato K, Tanami Y, Yun S, Sasaki K, Okano Y, Sugisawa K (2005) Quantitative evaluation of coronary arterial stenosis using 16-slice multidetector-row computed tomography: preliminary evaluation of phantom study. *J Comput Assist Tomogr* 29(3):382–386. <https://doi.org/10.1097/01.rct.0000161421.88001.f2>
 24. Vermiglio G, Acri G, Testagrossa B, Bramanti P, Bramanti A (2015) Universal phantom structure for quality inspections both on computerized tomography and on magnetic resonance tomography. Publication number: WO2015/092776 International Application No.: PCT/IB2014/067215
 25. Samavat H, Evans JA (2006) An ideal blood mimicking fluid for doppler ultrasound phantom. *J Med Phys* 31(4):275–278. <https://doi.org/10.4103/0971-6203.29198>
 26. King DM, Hangiandreou NJ, Tradup DJ, Stekel SF (2010) Evaluation of a low-cost liquid ultrasound test object for detection of transducer artefacts. *Phys Med Biol* 55:N557–N570. <https://doi.org/10.1088/0031-9155/55/23/N01>
 27. Dabrowski W, Dunmore-Buyze J, Rankin RN, Holdsworth DW, Fenster A (1997) A real vessel phantom for imaging experimentation. *Med Phys* 24(5):687–693. <https://doi.org/10.1118/1.597991>
 28. Den Hartog AG, Bovens SM, Koning W, Hendrikse J, Luijten PR, Moll FL, Pasterkamp G, de Borst GJ (2013) Current status of clinical magnetic resonance imaging for plaque characterisation in patients with carotid artery stenosis. *Eur J Vasc Endovasc Surg* 45(1):7–21. <https://doi.org/10.1016/j.ejvs.2012.10.022>
 29. Kwee RM, Truijman MTB, van Oostenbrugge RJ, Mess WH, Prins MH, Franke CL, Korten AGGC, Wildberger JE, Kooi ME (2012) Longitudinal MRI study on the natural history of carotid artery plaques in symptomatic patients. *PLoS ONE* 7(7):e42472. <https://doi.org/10.1371/journal.pone.0042472>
 30. Zhu J, Bornstedt A, Merkle N, Liu N, Rottbauer W, Ma G, Rasche V (2016) T2-prepared segmented 3D-gradient-echo for fast T2-weighted high-resolution three-dimensional imaging of the carotid artery wall at 3T: a feasibility study. *BioMed Eng OnLine* 15(Suppl 2):451–460. <https://doi.org/10.1186/s12938-016-0276-9>